BIOCHEMISTRY
including biophysical chemistry & molecular biology
Article

Biochemistry **2010,** *49,* 3619–3630 3619
DOI: 10.1021/bi100199q

Phosphorylation of the Transcription Factor Ets-1 by ERK2: Rapid Dissociation of ADP and Phospho-Ets-1[†]

Kari Callaway,[‡,@] William F. Waas,[‡,§] Mark A. Rainey,[‡,∥] Pengyu Ren,[⊥,∥] and Kevin N. Dalby*[,‡,§,@]

[‡]*Division of Medicinal Chemistry, University of Texas, Austin, Texas 78712,* [§]*Graduate Programs in Pharmacy,* [∥]*Cellular and Molecular Biology,* [⊥]*Biomedical Engineering, and* [@]*Biochemistry, University of Texas, Austin, Texas 78712*

Received February 9, 2010; Revised Manuscript Received April 1, 2010

ABSTRACT: ERK2, a major effector of the BRAF oncogene, is a promiscuous protein kinase that has a strong preference for phosphorylating substrates on Ser-Pro or Thr-Pro motifs. As part of a program to understand the fundamental basis for ERK2 substrate recognition and catalysis, we have studied the mechanism by which ERK2 phosphorylates the transcription factor Ets-1 at Thr-38. A feature of the mechanism in the forward direction is a partially rate-limiting product release step ($k_{off} = 59 \pm 6\ s^{-1}$), which is significant because to approach maximum efficiency substrates for ERK2 may evolve to ensure that ADP dissociation is rate-limiting. To improve our understanding of the mechanism of product release, the binding of the products to ERK2 was assessed and the reaction was examined in the reverse direction. These studies demonstrated that phospho-Ets-1 (*p*-Ets) binds >20-fold more tightly to ERK2 than ADP ($K_d = 7.3$ and 165 μM, respectively) and revealed that the products exhibit little interaction energetically while bound to ERK2 and that they can dissociate ERK2 in a random order. The overall equilibrium for the reaction in solution ($K_{eq} = 250\ M^{-1}$) was found to be similar to that with the substrate bound to the enzyme ($K_{int} = 525\ M^{-1}$). To determine what limits k_{off}, several pre-steady-state experiments were performed. A catalytic trapping approach furnished a rate constant (k^a_{-ADP}) of $61 \pm 12\ s^{-1}$ for the dissociation of ADP from the abortive ternary complex, ERK2·Ets·ADP. To examine *p*-Ets dissociation, the binding of a fluorescent derivative (*p*-Ets-*F*), which binds ERK2 with an affinity similar to that of *p*-Ets, was examined by stopped-flow kinetics. Using this approach, *p*-Ets-*F* was found to bind through a single-step mechanism, with the following parameters: $k_{-p\text{-Ets-}F} = 121 \pm 3.8\ s^{-1}$, and $k_{p\text{-Ets-}F} = (9.4 \pm 0.3) \times 10^6\ M^{-1}\ s^{-1}$. Similar results were found in the presence of a saturating ADP concentration. These data suggest that k_{off} may be limited by the dissociation of both products and are consistent with the notion that Ets-1 has evolved to be an efficient substrate for ERK2, where ADP release is, at least, partially rate-limiting. A molecular mechanics model of the complex formed between ERK2 and residues 28−138 of Ets-1 provides insight into the role of substrate docking interactions.

The therapeutic potential of targeting the Ras pathway has been recognized (*1*−*5*) and could be the single most important mitogenic pathway in human cells, contributing to more than 30% of all known cancers (*6*). Ras, a GTPase, is anchored to the cytoplasmic face of the plasma membrane and is activated by a cascade of events following the binding of various hormones to their respective cell surface receptors. Unregulated signaling from growth factor receptors and oncogenic forms of Ras and the Ras effector protein kinase Raf (*7*−*12*) lead to sustained ERK1 and ERK2 activity, which results in the unrestricted activation of signals that control cell survival and/or progression into the S phase of the cell cycle (*13*, *14*). A recent study identified mutant RAS and BRAF in cancer cell lines of various origins and showed that BRAF oncogenic mutations occur in approximately 8% of human cancers, being particularly common in melanoma, colon cancer, and non-small lung carcinoma (*15*).

ERK1 and ERK2 are remarkable enzymes, each displaying an ability to efficiently phosphorylate a subset of Ser/Thr-Pro motifs residing on various cellular proteins. Notably, they display an ability to discriminate against many accessible Ser/Thr-Pro motifs, while rapidly phosphorylating others. The specificity of ERK1 and ERK2 for their substrates is achieved, in part, through the utilization of remote recruitment sites. For example, ERK2 has two recruitment sites that are used to bind short peptide motifs (*16*) called the D-recruitment site (DRS)[1] and the F-recruitment site (FRS) (please see Figure 1A).

While the importance of the DRS and FRS in recognizing ERK2 substrates is well-established, general principles governing

[†]This research was supported in part by grants from the Welch Foundation (F-1390) to K.N.D. and the National Institutes of Health to K.N.D. (GM59802) and P.R. (GM79686).

*To whom correspondence should be addressed: Division of Medicinal Chemistry, College of Pharmacy, University of Texas, Austin, TX 78712. Telephone: (512) 471-9267. Fax: (512) 232-2606. E-mail: Dalby@mail.utexas.edu.

[1]Abbreviations: BSA, bovine serum albumin fraction V; DTT, dithiothreitol; EDTA, ethylenediaminetetraacetic acid; EGTA, ethylene glycerol bis(2-aminoethyl ether)-*N*,*N*,*N*′,*N*′-tetraacetic acid; IAA, iodoacetamide; TPCK, tosylphenylalanylchloromethane; HEPES, *N*-(2-hydroxyethyl)-piperazine-*N*′-2-ethanesulfonic acid; TRIS, tris(hydroxymethyl)aminomethane; IPTG, isopropyl β-D-thiogalactopyranoside; PMSF, phenylmethanesulfonyl fluoride; TFA, trifluoroacetic acid; ERK, extracellular signal-regulated protein kinase; Ets, murine (His_6-tagged) Ets-1(1−138); *p*-Ets, murine (His_6-tagged) Ets-1(1−138) phosphorylated at Thr-38; *p*-Ets-*F*, murine (His_6-tagged) Ets-1(1−138) containing a single Cys residue at position 31 labeled with 5′-iodoacetamidofluorescein phosphorylated at Thr-38; MAPK, mitogen-activated protein kinase; PCR, polymerase chain reaction; ESI, electrospray ionization; DRS, D-recruitment site; FRS, F-recruitment site; MKK1G7B, constitutively active recombinant human mitogen-activated protein kinase kinase 1 (ΔN4/S218D/M219D/N221D/S222D, where ΔN4 indicates a deletion of residues 32−43); SAM, sterile α motif; PDB, Protein Data Bank.

Published on Web 04/02/2010

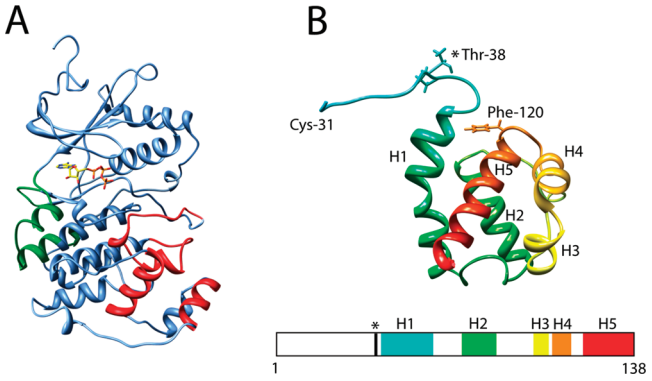

FIGURE 1: (A) Ribbon representation showing the structural features of MKK1-activated ERK2. The D-recruitment site (colored green) is comprised of the reverse turn (Asn-156−Asp-160) between sheet β7 and sheet β8, part of loop 7 (Glu-107−Asp-109), helix αD (Leu-110−Thr-116), loop 8 (Gln-117−Ser-120), and part of helix αE (Asn-121−Phe-127) and the common docking domain (Asp-316 and Asp-319). For the F-recruitment site (colored red), this pocket shows a preference for aromatic residues at positions P + 6 and P + 8. The pocket is comprised of the C-terminus of the activation segment starting at Phe-181 through the end of loop 12 (Phe-181−Thr-204), helix αG (Tyr-231−Leu-242), and α2L14 of the MAPK insert helix (Leu-256−Leu-263). The structure corresponds to PDB entry 2ERK. The ATP molecule is superimposed on the structure following alignment with PKA in PDB entry 1ATP. (B) Ribbon representation of residues 31−138 of Ets-1 (PDB entry 2JV3). The ERK2 phosphorylation site, Thr-38, is shown as well as Phe-120, a residue implicated in ERK2 binding. The five helices, H1−H5, that comprise the SAM domain of Ets-1 are shown.

mechanisms of substrate recognition and turnover by ERK2 remain to be elucidated. For example, there is no clear understanding of the relationships between docking interactions at the recruiting sites and events, such as phosphorylation, that occur within the active site. It is also not known whether all docking interactions function through similar mechanisms.

To address some of these questions, we examined the mechanism of phosphorylation of the transcription factor Ets-1 (which lacks a conventional DRS and FRS) by ERK2, using residues 1−138 as a surrogate of the full-length protein.[2] The N-terminus (residues 1−39) of Ets-1 is disordered, while residues 40−138, including a sterile α motif (SAM) domain (*18*), form a five-helix bundle, with helix 1 beginning immediately *C*-terminal to the phosphorylation site Thr-38 (Figure 1B).[3] ERK2 catalyzes the phosphorylation of Ets-1 at Thr-38 with remarkable specificity (*19*, *20*). Structure−function studies suggest that both the N-terminus and the SAM domain of Ets-1, but not the Thr-Pro motif, contribute to the formation of the ERK2−Ets complex (*21*, *22*), thereby bringing Thr-38 into the proximity of the active site, to facilitate phosphorylation of Thr-38, through a mechanism

Scheme 1: [a]

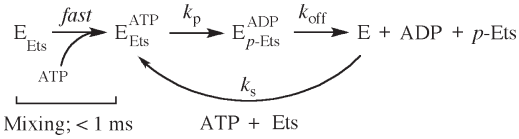

[a]In rapid quench experiments, ERK2 and Ets are pre-incubated in standard assay buffer to form the binary complex, E_{Ets}, before being rapidly mixed with ATP to form the ternary complex, E_{Ets}^{ATP}. This complex undergoes phosphorylation, k_p, followed by product release, k_{off}. In the presence of excess substrates, the conversion of free E to the ternary substrate complex, k_s, is assumed to be rapid.

termed proximity-induced catalysis (*23*).[4] This mechanism was proposed because Ets binds unactivated ERK2 (which lacks the ability to bind the Thr-Pro motif) with an affinity similar to that of activated ERK2 (*21*). Furthermore, mutation of Pro-39 to bulky or charged residues has no significant effect on the affinity of the Ets protein for ERK2 in the absence and presence of an ATP analogue (*23*). These results suggest that the binding of the Thr-Pro motif in the active site of ERK2 is not essential for complex formation.

Kinetic studies revealed that the turnover of Ets-1 by ERK2 is governed by two partially rate-limiting steps, which are attributed to the phosphorylation of Ets-1 on the enzyme (k_p = 106 ± 8 s^{-1}) and the process of product release (k_{off} = 59 ± 6 s^{-1}) (Scheme 1) (*24*). Here we examine the mechanism of product release in more detail to address whether this step is limited by the dissociation of ADP or phospho-Ets. This study is significant, because it addresses the notion that substrates for a promiscuous protein kinase such as ERK2 likely evolve to rapidly dissociate once phosphorylated. To address the mechanism, we examined the reaction using a combination of steady-state and pre-steady-state kinetics.

EXPERIMENTAL PROCEDURES

Reagents. Ultrapure grade Tris and HEPES were obtained from ICN Biomedicals (Aurora, OH). 5′-Iodoacetamidofluorescein (5-IAF) was purchased from Molecular Probes (Eugene, OR). 5,5′-Dithiobis(2-nitrobenzoic acid) and all other chemicals were from Sigma (St. Louis, MO). Perkin Elmer supplied [γ-^{32}P] ATP. P81 Ion Exchange Cellulose Chromatography Paper was purchased from Whatman. *Escherichia coli* strain DH5α, used for cloning and isolation of plasmids, was obtained from Invitrogen Corp. (Carlsbad, CA). *E. coli* strain BL21(DE3), used for recombinant protein expression, was purchased from Novagen (Madison, WI). Tryptone, yeast extract, and agar were obtained from US Biologicals (Swampscott, MA) and BD (Sparks, MD), respectively. The Mono-Q HR 10/10 anion exchange column and PD-10 desalting columns were purchased from Amersham Biosciences (Piscataway, NJ). Qiagen Inc. (Valencia, CA) supplied the Ni-NTA agarose and the Qiaprep Spin miniprep kit. Ambion, Inc. (Austin, TX), provided the thin-walled PCR tubes. Restriction enzymes, PCR reagents, and T4 DNA ligase were from Hoffmann-La Roche, Ltd. (Basel, Switzerland), Promega Corp. (Madison, WI), or New England Biolabs (Beverly, MA). Oligonucleotides for DNA amplification and sequencing were from Genosys (The Woodlands, TX). The remaining molecular biology reagents, including DNA ladders and protein molecular mass standards, were obtained from Invitrogen Corp.

[2]Residues 1−138 of Ets-1, which we term Ets for the sake of convenience, are an excellent model for the full-length Ets-1 protein with respect to its recognition and phosphorylation by ERK2 (*17*).

[3]An NMR-derived structure of Ets was recently updated as PDB entry 2JV3.

[4]MAP kinases phosphorylate substrates within a consensus sequence, φ-χ-Ser/Thr-θ, where φ corresponds to a small hydrophobic residue (often proline), χ corresponds to any amino acid, and θ corresponds to proline. Recognition of the consensus sequence by the MAPK is mediated by intrinsic interactions mainly involving the activation segment of the MAPK. However, according to the mechanism of proximity-induced catalysis, the consensus sequence of Ets-1 neither contributes binding energy nor interacts intimately with the active site of ERK2 in the ground-state ternary complex. Rather, the ternary complex is stabilized exclusively by interactions extrinsic to the active site, which are often termed docking interactions.

Preparation of Proteins. The expression of MKK1G7B, ERK2, Ets, and Ets-*F* and the activation of ERK2 by MKK1G7B have been reported previously (*21*).

Phosphorylation of Ets and Ets-F. Purified Ets or Ets-*F* (20 μM) was incubated with active ERK2 (5 nM) at 27 °C in 50 mM HEPES (pH 7.4), 100 mM KCl, 2 mM DTT, 0.1 mM EDTA, 0.1 mM EGTA, 40 μg/mL BSA, 10 mM $MgCl_2$, and 2 mM ATP (3 mL of buffer/mg of protein) for 2 h. The reaction was stopped with 10 mM EDTA, and the ATP was removed by dialysis in 20 mM Tris (pH 8.0), 0.1% (v/v) β-mercaptoethanol, and 0.3% (by mass) Brij-30. Following dialysis, the protein was purified by anion exchange chromatography on a Mono-Q HR 10/10 column that was developed with a gradient from 0 to 500 mM NaCl over 17 column volumes. After the protein was eluted at 250 mM NaCl, the selected fractions were combined and dialyzed in 25 mM HEPES (pH 7.5), 50 mM KCl, 2 mM DTT, 0.1 mM EDTA, and 0.1 mM EDTA. The phosphorylation of Ets and Ets-*F* was confirmed by ESI mass spectrometry following elution (0 to 100% acetonitrile, 80 min, 0.6 mL/min) from a reverse phase C18 Vydac column (218TP54, 25 cm × 4 mm).

Molecular Biology. A bacterial expression vector, NpT7-5, encoding a hexahistidine tag followed by cDNA encoding rat ERK2 (NpT7-5 His_6-ERK2, a gift of N. Ahn, University of Colorado, Boulder, CO), was modified by PCR using site-directed mutagenesis to construct K229T/H230D ERK2. The NpT7-5 His_6-ERK2 vector was digested with SacII and HindIII and ligated into a SacII−HindIII-digested pBluescript (pBS) vector using T4 DNA ligase to create pBS-ERK2. The mutations were produced by a two-step PCR using the following conditions: 94 °C for 5 min to denature the complementary strands; 30 cycles of 55 °C for 30 s to anneal the primers, extension for 1 min at 72 °C, followed by a denaturation step at 94 °C for 45 s; complementary strands extended for a final 10 min at 72 °C. The first round of PCR generated two overlapping products, fragments A and B, from two separate reactions using pBS-ERK2 as the template. Fragment A was amplified using an outer forward primer that contained an EcoRI restriction site (underlined) (5′-TAT GTT GAA TTC CAA GGG TTA TAC-3′) and an inner reverse primer containing the K229T/H230D mutation (italics) (5′-CTG GTC AAG GTA GTC *GGT TCC* TGG GAA GAT-3′). Fragment B was amplified with an inner forward primer containing the K229T/H230D mutation (5′-ATC TTC CCA *GGA ACC* GAC TAC CTT GAC CAG-3′) and an outer reverse primer containing the beginning of the HindIII restriction site in ERK2 (5′-GGT CGA CGG TAT CGA TAA GC-3′). Fragments A and B were purified and used as templates for a second round of PCR using only the outer primers. The product was digested with EcoRI and HindIII and ligated into EcoRI−HindIII-digested pBS-ERK2. The pBS-ERK2 mutants were digested with SacII and HindIII and subcloned into SacII−HindIII-digested NpT7-5 His6-ERK2. All mutations were verified by sequencing the DNA at University of Texas core facilities.

Ligand Binding. (*i*) *Isothermal Titration Calorimetry*. Prior to the experiment, active ERK2 was dialyzed into 25 mM HEPES (pH 8.0), 100 mM KCl, 2 mM β-mercaptoethanol, and 20 mM $MgCl_2$. To ensure that the buffer was identical, the dialysis buffer was then used to make the MgADP solution. The concentration of the MgADP solution was such that a 2.5 molar ratio of MgADP to active ERK2 was reached in the cell upon the last injection. Titrations were conducted on a MCS titration calorimeter (Microcal, Inc.) at 27 °C in 25 mM HEPES (pH 8.0), 100 mM KCl, 2 mM β-mercaptoethanol, and 20 mM $MgCl_2$. ADP was titrated into 263 μM ERK2 with one 2 μL injection followed by 25 injections (10 μL each) with a 5 s injection duration followed by 240 s between injections. Control experiments used the same buffer as the experiments but were conducted in the absence of ERK2. The data resulting from the control experiment were subtracted from the experimental data using Origin version 2.3. This same software was used for integrations and fitting to a simple one-binding site model. The data fitting process produced values for the binding stoichiometry (n), association constant (K_a), and molar change in enthalpy (ΔH).

(*ii*) *Fluorescence Anisotropy Binding Assays*. Assays were performed as previously described (*21*).

Kinetic Experiments. (*i*) *Steady-State Kinetic Experiments in the Reverse Direction*.[5] Reactions were conducted at 27 °C in kinase assay buffer [25 mM HEPES (pH 7.4), 100 mM KCl, 2 mM DTT, 40 μg/mL BSA, and 20 mM $MgCl_2$] containing 50 nM ERK2 and varied concentrations of [^{32}P]-*p*-Ets (1.8−90 μM) and ADP (100−5000 μM). Rates were measured under conditions where total product formation represented less than 10% of the initial substrate concentrations. The reaction mixture was incubated for 10 min before initiation by addition of enzyme. Aliquots (8 μL) were taken at time points and applied to a 20 cm × 20 cm silica gel thin-layer chromatography (TLC) plate (Sigma, St. Louis, MO). TLC plates were developed in TLC eluent [300 mM ammonium acetate, 366 mM HCl, and 20% (v/v) methanol] and exposed to Phosphor screens (Molecular Dynamics). The amount of [γ-^{32}P]ATP formed was determined using ImageQuant (Molecular Dynamics) and calibration with a sample of known specificity. Initial rates were determined by linear least-squares fitting to plots of product versus time. We obtained the kinetic constants using Scientist (Micromath) by fitting the data to eq 1 by global fitting.

$$k_{obs} = \frac{k_{cat}[ADP][p\text{-Ets}]}{K_m^{ADP}K_m^{p\text{-Ets}} + K_m^{p\text{-Ets}}[ADP] + K_m^{ADP}[p\text{-Ets}] + [ADP][p\text{-Ets}]} \quad (1)$$

(*ii*) *Rapid Chemical Quench*.[6] Rapid quench experiments were performed on a KinTek RQF-3 rapid quench-flow apparatus. Reactions were conducted at 27 °C in 25 mM HEPES (pH 8.0), 50 mM KCl, 2 mM DTT, and 20 mM $MgCl_2$. Experiments were initiated by the rapid mixing of solution A (containing ERK2) with an equal volume of solution B

[5]Steady-state kinetic terms: k_{cat}^{f} and k_{cat}^{r}, catalytic constants for forward and reverse reactions, respectively; K_m^{ADP}, K_m^{ATP}, K_m^{Ets}, and $K_m^{p\text{-Ets}}$, Michaelis−Menten constants for ADP, ATP, Ets, and *p*-Ets, respectively; K_d^{ADP} and $K_d^{p\text{-Ets}}$, dissociation constants for the dissociation of ADP and *p*-Ets from E^{ADP} and $E_{p\text{-Ets}}$, respectively; K_i^{ATP} and K_i^{Ets}, inhibition constants for ATP and Ets, respectively; k_p and k_{-p}, first-order rate constants for the interconversion of the K_{Ets}^{ATP} and $K_{p\text{-Ets}}^{ADP}$ ternary complexes in the forward and reverse direction, respectively; K_{eq}, equilibrium constant for the forward reaction between ATP and Ets in solution; K_{int}, equilibrium constant for the forward reaction between ATP and Ets while bound to ERK2.

[6]Pre-steady-state kinetic terms: k_{off}, first-order rate constant for the formation of E from $E_{p\text{-Ets}}^{ADP}$; k_{-ADP}, first-order rate constant for the dissociation of ADP from E^{ADP}; k_{-ADP}^{a}, first-order rate constant for the dissociation of ADP from the abortive complex E_{Ets}^{ATP}; $k_{-p\text{-Ets}}$, first-order rate constant for the dissociation of *p*-Ets from $E_{p\text{-Ets}}$; $k_{+p\text{-Ets}}$, second-order rate constant for the association of *p*-Ets and ERK2; $k_{-p\text{-Ets-}F}$, first-order rate constant for the dissociation of *p*-Ets-*F* from $E_{p\text{-Ets-}F}$; $k_{+p\text{-Ets-}F}$, second-order rate constant for the association of *p*-Ets-*F* and ERK2; k_s, rate constant for the recombination of substrates with free ERK2.

(containing other reagents, including ATP). After brief time intervals (2−100 ms), reactions were quenched with 115 μL of 2 M H_3PO_4. The quenched reaction mixture was collected in 1.5 mL centrifuge tubes and centrifuged briefly at 5000*g*. Aliquots (50 μL) of the quenched reaction mixture were spotted on P81 paper. The papers were washed first in 50 mM H_3PO_4 (3 × 10 min) and then in acetone (3 × 1 min). After the papers were dry, the amount of *p*-Ets was determined by counting the associated counts per minute on a scintillation counter. Data were fitted by global fitting by numerical integration to the appropriate kinetic model using KinTek Explorer Pro (*25*, *26*).

(*iii*) *Fluorescence Stopped Flow*. Stopped-flow measurements were performed on a KinTek SF 2001 Airforce 1 air-driven stopped-flow apparatus. To establish the dead time, the fluorescence quenching of *N*-acetyltryptophanamide by *N*-bromosuccinimide was monitored (*27*). For the KinTek SF 2001 Airforce 1 stopped-flow instrument, a dead time of 2 ms was determined. Experiments were conducted at 27 °C using 530 nm band-pass filters with a 25 nm bandwidth (Corion). An excitation wavelength of 492 nm was used. A 200 nM solution of *p*-Ets-*F* in 25 mM HEPES (pH 7.5), 50 mM KCl, 2 mM DTT, 40 μg/mL BSA, 0.1 mM EDTA, and 0.1 mM EGTA was reacted with solutions of ERK2 (1−40 μM) in the same buffer. The solutions were incubated at 27 °C for 3 min before being mixed to give final concentrations of 100 nM *p*-Ets-*F* and 0.5−20 μM ERK2. The reaction was monitored for a total of 30 ms, and an average of four or five traces was used for data analysis. Data were fitted by numerical integration to the appropriate kinetic model using KinTek Explorer Pro (*25*, *26*).

Modeling for ERK2−Ets 28−138 Interactions. The complex structure of active ERK2 (PDB entry 2ERK) and Ets (PDB entry 2JV3) was predicted using the molecular mechanics modeling approaches available in TINKER (*28*). An OPLS-AA force field (*29*) was used to represent atomic interactions. Regular unphosphorylated Thr and Tyr residues replaced the phosphorylated Thr and Tyr residues in PDB entry 2ERK. The two molecules were first separated by 40 Å, with the ERK2 active site facing the N-terminus of Ets. The potential smoothing (PSS) method (*30*) was then used to "dock" the two proteins into a complex by minimizing the total system energy. During the energy minimization, ERK2 was kept rigid, and so was Ets except for N-terminal residues 29−53. To allow for backbone conformational changes in the N-terminal segment of Ets, residues 29−53 of Ets were divided into rigid bodies comprised of backbone amides and side chain groups (i.e., each residue containing two rigid bodies). In PSS, a smoothing parameter of 20 was utilized, with 100 steps in the smoothing schedule. Energy minimization ceased when the energy gradient dropped below 0.1 kcal/mol per degree of freedom. The nonbonded interactions were cut off at 30 Å. A dielectric constant of 5 was used. To facilitate the search for optimal complex structure, a flat bottom restraint was applied between the C_β atom of Thr-38 in Ets and the C_γ atom of Asp-147 in ERK2. The restraint (K_r = 2.0 kcal mol^{-1} Å^{-2}) worked to loosely pull the two atoms into each other's proximity (2−6 Å).

The PSS-minimized structure was then subjected to atomic energy minimization (without the rigid body constraint) using the GBSA implicit solvent model. The conformation of the ^{38}Thr-Pro^{39} motif is inferred from the known conformation of the peptide substrate in the CDK active site (PDB entry 1QMZ). To take advantage of this known conformation, additional restraints were applied to force the ^{38}Thr-38-Pro^{39} motif to adopt the corresponding backbone torsion angles found in the CDK2·peptide complex in PDB entry 1QMZ, and also to push Pro-39 into the hydrophobic pocket behind phospho-Tyr-185 of ERK2. The overall structural change [root-mean-square deviation (rmsd)] caused by this minimization is less than 0.5 Å, mostly in the N-terminus of Ets where the restraints were applied. The effect on the ERK2−Ets interface away from the active site was negligible. All restraints were then removed for another fully atomic energy minimization, in which all degrees of freedom were set free, again in the GBSA implicit solvent.

Scheme 2: Random-Order Ternary Complex Mechanism Involving Two Abortive Complexes in the Forward and Reverse Direction

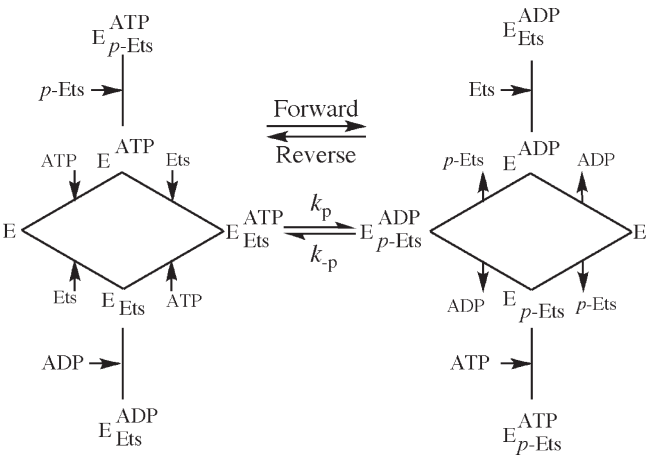

Electrospray Ionization Mass Spectrometry of Proteins and Peptides. Proteins and tryptic peptides were analyzed by an electrospray ion trap mass spectrometer (LCQ, Finnigan MAT, San Jose, CA) coupled online with a microbore HPLC system (Magic 2002, Michrom BioResources, Auburn, CA). A 10 μL sample of the protein was injected into a microbore HPLC system, and the protein was eluted with a 0.5 mm × 50 mm PLRP-S column (8 μm particle diameter, 4000 Å pore size; Michrom BioResources) with mobile phase A (2/98/0.1/0.02 acetonitrile/water/acetic acid/trifluoroacetic acid mixture) and B (90/10/0.09/0.02 acetonitrile/water/acetic acid/trifluoroacetic acid mixture). The gradient used to elute protein was from 5 to 95% mobile phase B over 10 min followed by 95% B for 5 min at a flow rate of 20 μL/min. Automated acquisition of full scan MS spectra was achieved with Finnigan Excalibur. The settings for ESI were as follows: spray voltage, 4.5 kV; nitrogen sheath gas and auxiliary gas flow rates, 60 and 5 psi, respectively; capillary temperature, 200 °C; capillary voltage, 22 V; tube lens offset, 40 V. The electron multiplier was set at −860 V; the scan time setting was performed with 50 ms of max injection time for full scan. The target number of ions for MS was 1 × 10^8. The full scan range for MS was 300−2000 Da. The Finnigan-MAT BIOWORKS software to afford the MH$^+$ *m*/*z* value(s) of the protein sample deconvoluted the acquired convoluted protein spectra from LCQ.

RESULTS

Kinetic Mechanism of ERK2 in the Reverse Direction. To begin an investigation into the mechanism of product release, we first examined the reaction in the reverse direction, which has the potential to provide a measure of the reversibility of the reaction as well as insight into the interactions of the product ADP and *p*-Ets while bound to ERK2. We have previously

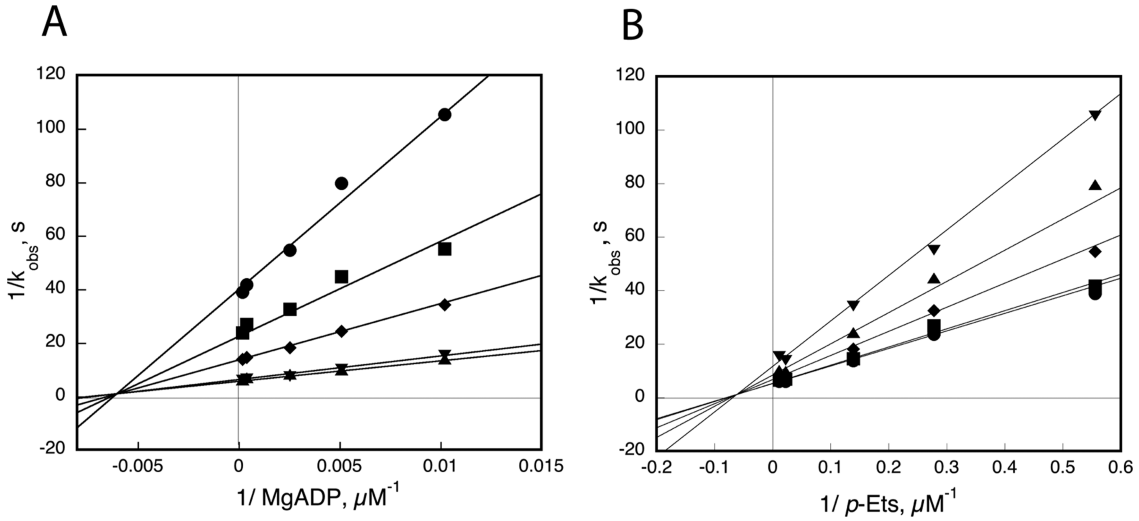

FIGURE 2: Reverse reaction initial velocity studies. Reactions were performed at 27 °C in kinase assay buffer [25 mM HEPES (pH 7.4), 2 mM DTT, 40 μg/mL BSA, and 20 mM $MgCl_2$]. The ionic strength was maintained at 150 mM with KCl. Initial velocities were measured using ERK2 (50 nM), *p*-Ets (1.8−90 μM), and ADP (0.1−5 mM). The data were fitted to eq 1 and used to create reciprocal plots for (A) ADP at varied fixed concentrations of *p*-Ets [1.8 (●), 3.6 (■), 7.2 (◆), 45 (▼), and 90 μM (▲)] and (B) *p*-Ets at varied fixed concentrations of ADP [100 μM (▼), 200 μM (▲), 400 μM (◆), 2.5 mM (■), and 5 mM (●)]. The parameters are listed in Table 1.

Table 1: Steady-State Kinetic and Thermodynamic Parameters

parameter	value	parameter	value
k_{cat}^{r}	0.2 ± 0.03 s^{-1} [a]	$K_d^{p\text{-Ets}}$	16.0 ± 3 μM [a]
K_m^{ADP}	130.0 ± 18 μM [a]	k_{cat}^{f}	17.0 ± 3.0 s^{-1} [d]
K_d^{ADP}	165.0 ± 19 μM [a]	K_m^{ATP}	140.0 ± 5.0 μM [d]
K_d^{ADP}	172.0 ± 6 μM [b]	K_i^{ATP}	65.0 ± 5.0 μM [d]
$K_m^{p\text{-Ets}}$	13.0 ± 1 μM [a]	K_m^{Ets}	18.0 ± 2.0 μM [d]
$K_d^{p\text{-Ets}}$	7.3 ± 0.5 μM [c]	K_i^{Ets}	9.0 ± 1.0 μM [d]

[a]Initial velocities were measured using 50 nM ERK2, 20 mM $MgCl_2$, 2 mM DTT, 0.1−5 mM ADP, and 1.8−90 μM *p*-Ets (pH 7.4) at 27 °C with an ionic strength of 0.15 M (KCl). [b]Determined by isothermal calorimetry. [c]Determined by a fluorescence anisotropy competition assay. [d]Initial velocities were measured using 2 nM ERK2, 20 mM $MgCl_2$, 2 mM DTT, 32−710 μM ATP, and 5.5−100 μM Ets (pH 7.5) at 27 °C with an ionic strength of 0.1 M (KCl).

examined the kinetic mechanism of ERK2 in the forward direction by initial velocity measurements in both the absence and presence of products and shown it to be a random-order ternary complex mechanism with the formation of two abortive complexes (Scheme 2). The reverse reaction was studied by following the phosphorylation of ADP, using ^{32}P-labeled *p*-Ets as the phosphate donor. *p*-Ets is readily prepared by incubation of Ets with ATP in the presence of ERK2 (*20*). Initial velocity studies were performed using 50 nM ERK2, varied concentrations of ADP (100−5000 μM) and [^{32}P]-*p*-Ets (1.8−90 μM) under buffer conditions identical to those used to study the reaction in the forward direction (*20*) [e.g., 27 °C, 25 mM HEPES (pH 7.4), 100 mM KCl, 2 mM DTT, 40 μg/mL BSA, and 20 mM $MgCl_2$]. By applying aliquots of each reaction mixture to thin layer chromatography plates and developing the plates in acidic 20% methanol, we were able to conveniently monitor the formation of [γ-^{32}P]ATP over the course of the reaction. Quantification of reaction progress was then achieved by determination of the amount of ^{32}P associated with the migrating ATP using a phosphorimager (see Experimental Procedures). The observed rate constants, k_{obs}, were generally reproducible within 10%. The resulting experimental data were used to create plots of $1/k_{obs}$ versus 1/[ADP] or 1/[*p*-Ets] (Figure 2A,B). In both cases, reciprocal plots clearly intersect to the left of the ordinate and above the abscissa, consistent with a sequential mechanism (*31*). Analysis of the data according to eq 1 provided the kinetic parameters listed in Table 1. Several features of these parameters are notable. For example, the Michaelis constants for Ets and *p*-Ets (K_m^{Ets} = 18 μM, and $K_m^{p\text{-Ets}}$ = 13 μM) are similar, suggesting that the phosphorylation of Ets has little effect on its ability to bind ERK2.

Kinetic Mechanism of p-Ets Binding. To evaluate the mechanism of *p*-Ets binding, a fluorescent derivative called *p*-Ets-*F* was utilized, which contains a single fluorescein-labeled cysteine at position 31 (*21*). To evaluate the binding of *p*-Ets-*F* to ERK2, we adopted a fluorescence anisotropy approach used previously to assess the binding of Ets to ERK2 (*21*). Assays were performed in 25 mM HEPES (pH 7.5), 50 mM KCl, 20 mM $MgCl_2$, 40 μg/mL BSA, 0.1 mM EDTA, 0.1 mM EGTA, 1.3% glycerol, and 2 mM DTT containing ERK2 (0−20 μM) and 100 nM *p*-Ets-*F* in a final volume of 60 μL. Fluorescence anisotropy measurements were taken at 27 °C using a Fluorolog model FL3-11 fluorometer (Jobin Yvon, Edison, NJ). Thus, a 100 nM solution (final concentration) of *p*-Ets-*F* was added to varying concentrations of activated ERK2 and the resulting anisotropy determined (Figure 3B). As expected, the anisotropy values increased upon the addition of ERK2, consistent with the formation of a *p*-Ets-*F*·ERK2 complex. As reported previously, activated ERK2 is monomeric under the assay conditions (*21*); therefore, the binding model shown in Scheme 3A is assumed. When the data are fit to eqs 2 and 3,[7] a dissociation constant

[7]Parameters for fluorescence binding: r_f and r_b, anisotropies of the free and bound fluorescein-labeled protein, respectively; *R*, ratio of fluorescent yields of the bound form and the free form of fluorescein-labeled protein S; $[S_t]$, $[B_t]$, and $[E_t]$, total concentrations of *p*-Ets-*F*, *p*-Ets, and ERK2, respectively; $[S_f]$, $[B_f]$, and $[E_f]$, concentrations of unbound forms of *p*-Ets-*F*, *p*-Ets, and ERK2, respectively; I_v and I_H, intensities of the emission at polarizations both parallel and perpendicular to the excitation source, respectively; *G*, factor to correct for instrumental differences in detecting emission components. Specifically, the *G* factor is the ratio of the intensity of the vertically and horizontally polarized emission components when the sample is excited with horizontally polarized light. Note *R* was determined to be 0.5 by measuring the fluorescence emission spectrum of *p*-Ets-*F* when bound to ERK2.

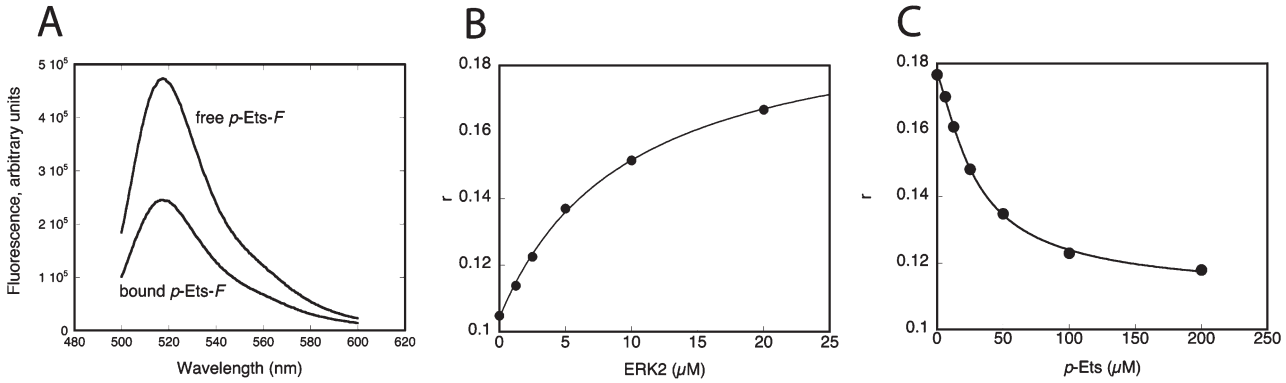

FIGURE 3: Binding of *p*-Ets-*F*. Binding assays were performed in 25 mM HEPES (pH 7.5), 50 mM KCl, 40 μg/mL BSA, 0.1 mM EDTA, 0.1 mM EGTA, 1.3% glycerol, and 2 mM DTT. (A) The fluorescence emission spectrum of 100 nM *p*-Ets-*F* was examined in the absence and presence of 20 μM active ERK2. The sample was excited with light at 492 nm, and an emission scan was performed from 500 to 600 nm. (B) Binding of 100 nM *p*-Ets-*F* to active ERK2 (0−20 μM). Anisotropy values were averaged, and the dissociation constants were determined by fitting the average anisotropy values to eq 3, according to Scheme 3A using Kaleidagraph 4.0 (Synergy software), where an *R* value of 0.5 was used. The best fit through the data furnished a $K_d^{p\text{-Ets-}F}$ value of 4.8 ± 0.5 μM. (C) A fluorescence anisotropy competition assay was performed with 100 nM *p*-Ets-*F*, 10 μM active ERK2, and varied *p*-Ets concentrations (0−200 μM). The experimental data were simultaneously fit to eqs 4−8 using an *R* value of 0.5 to give a $K_d^{p\text{-Ets}}$ value of 7.3 ± 0.5 μM.

Scheme 3: Binding Equilibria

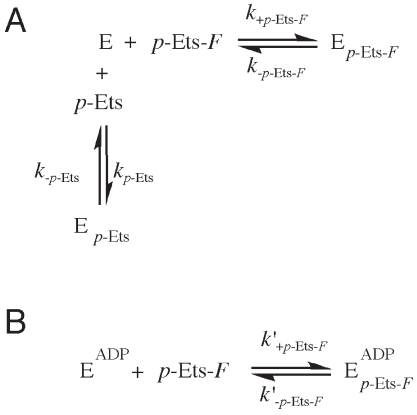

($K_d^{p\text{-Ets-}F}$) of 4.8 ± 0.5 μM was obtained for the binding of *p*-Ets-*F* to activated ERK2.

$$R = \frac{(I_v + 2GI_H)_{bound}}{(I_v + 2GI_H)_{free}} \quad (2)$$

$$r = (\{[K_d^{p\text{-Ets-}F} + [S_t] + [E_t] - \sqrt{(-K_d^{p\text{-Ets-}F} - [S_t] - [E_t])^2 - 4[E_t][S_t]}]/(2[S_t])\}[(r_b R - r_f) + r_f])/(1 + \{[K_d^{p\text{-Ets-}F} + [S_t] + [E_t] - \sqrt{(-K_d^{p\text{-Ets-}F} - [S_t] - [E_t])^2 - 4[E_t][S_t]}]/(2[S_t])\}(R-1)) \quad (3)$$

The binding affinity of *p*-Ets was then determined using a competition approach, according to Scheme 3A, previously used to assess the binding of Ets and PEA15 to ERK2 (*21*, *32*). Thus, a solution containing a fixed concentration of *p*-Ets-*F* and active ERK2 was added to a solution containing varied concentrations of *p*-Ets. As expected, there is a decrease in the final anisotropy reading with increasing concentrations of *p*-Ets, indicating that *p*-Ets competes with *p*-Ets-*F* for binding to active ERK2 (Figure 3C). Simultaneous fitting of the data to the five equations describing the equilibria in Scheme 3A (eqs 4−8) furnishes a single best fit for the dissociation constant $K_d^{p\text{-Ets}}$ of 7.3 ± 0.5 μM.

$$r = \frac{\frac{[ES]}{[S_t]}(r_b R - r_f) + r_f}{1 + \frac{[ES]}{[S_t]}(R-1)} \quad (4)$$

$$[ES] = \frac{[E_f][S_t]}{K_d^{p\text{-Ets-}F} + [E_f]} \quad (5)$$

$$K_d^{p\text{-Ets}} = \frac{[E_f][B_f]}{[EB]} \quad (6)$$

$$[B_t] = [B_f] + [EB] \quad (7)$$

$$[E_t] = [E_f] + [EB] \quad (8)$$

This anisotropy study suggested that *p*-Ets-*F* is a reasonable surrogate for assessing the interactions of *p*-Ets with ERK2, as the difference in the affinity of each protein for ERK2 is only 1.5-fold. During the course of the binding studies, we determined that the fluorescence emission of *p*-Ets-*F* decreases significantly when it binds to ERK2 (Figure. 3A). Therefore, a stopped-flow analysis was conducted at 27 °C to examine the mechanism of binding.

To measure the rate of *p*-Ets-*F* binding to ERK2, we used an excitation wavelength of 492 nm. Figure 4 shows representative experiments in which, in the presence of 20 mM Mg^{2+}, a solution of *p*-Ets-*F* (200 nM) was rapidly mixed with an equal volume of a solution containing either ERK2 (0−20 μM) alone (Figure 4A) or ERK2 (0−20 μM) and 8 mM ADP (Figure 4B). Each of the traces shown represents the average of five runs, and each was assessed in terms of several kinetic models, using the global fitting program KinTek Explorer Pro (*25*, *26*). In all cases, the best fit to the data corresponded to the single-step binding model shown in Scheme 3B. In the absence of ADP, the rate constants describing *p*-Ets-*F* binding are as follows: $k_{p\text{-Ets-}F}$ = (9.4 ± 0.3) × 10^6 M^{-1} s^{-1}, and $k_{-p\text{-Ets-}F}$ = 121 ± 4 s^{-1}. They correspond to a dissociation constant $K_d^{p\text{-Ets-}F}$ of 13 μM (Figure 4A), which is in

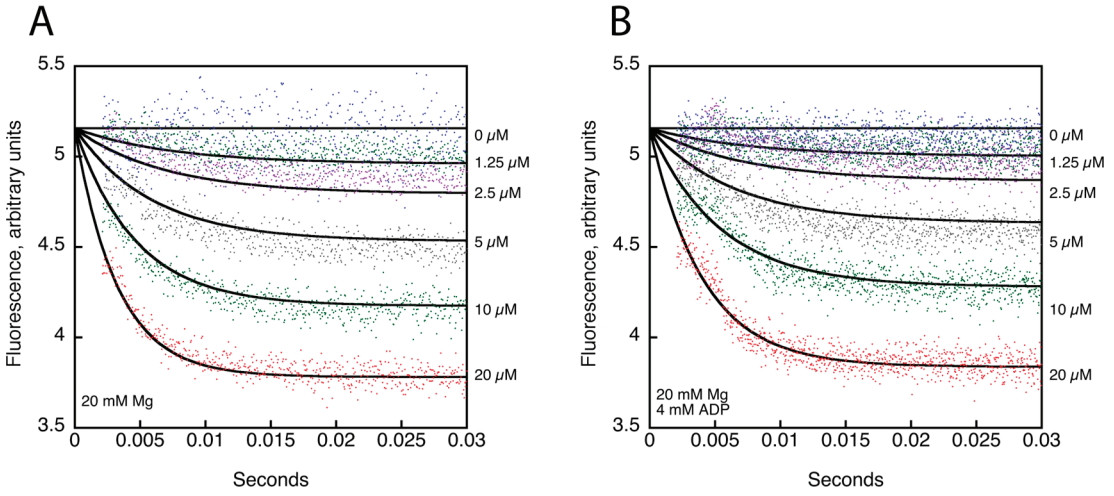

FIGURE 4: Fluorescence stopped-flow analysis of *p*-Ets-*F* binding to active ERK2. (A) In the absence of ADP. Stopped-flow experiments were conducted at 27 °C in 25 mM HEPES (pH 7.5), 50 mM KCl, 2 mM DTT, 40 μg/mL BSA, 0.1 mM EDTA, and 0.1 mM EGTA on a KinTek SF 2001 Airforce 1 stopped-flow apparatus fitted with 530 nm band-pass filters with a a 25 nm bandwidth (Corion). An excitation wavelength of 492 nm was used. Syringe A was loaded with a 200 nM solution of *p*-Ets-*F*. Syringe B was loaded with activated ERK2 (0−40 μM). The solutions were incubated at 27 °C for 3 min before being mixed to give final concentrations of 100 nM *p*-Ets-*F* and 0−20 μM ERK2. The reaction was monitored for a total of 30 ms, and an average of four or five traces was used for data analysis. Data were fitted by numerical integration to the single-step binding model in Scheme 3B using KinTek Explorer Pro (*25*, *26*) to give a $k_{+p\text{-Ets-}F}$ of $(9.4 \pm 0.3) \times 10^6$ M^{-1} s^{-1} and a $k_{-p\text{-Ets-}F}$ of 121 ± 3.8 s^{-1}. (B) In the presence of ADP. The experiment was performed as described for panel A, except syringe B was also loaded with 8 mM ADP, to give a final concentration after mixing of 4 mM ADP. Data were fitted by numerical integration to the model in Scheme 3B using KinTek Explorer Pro (*25*, *26*) to give a $k'_{+p\text{-Ets-}F}$ of $(6.2 \pm 0.2) \times 10^6$ M^{-1} s^{-1} and a $k'_{-p\text{-Ets-}F}$ of 123 ± 3 s^{-1}.

Table 2: Kinetic and Thermodynamic Parameters for the Binding of *p*-Ets-*F*

without ADP			with ADP		
$k_{+p\text{-Ets-}F}$ ($\times 10^6$ M^{-1} s^{-1})	$k_{-p\text{-Ets-}F}$ (s^{-1})	$K_d^{p\text{-Ets-}F}$ (μM)	$k'_{+p\text{-Ets-}F}$ ($\times 10^6$ M^{-1} s^{-1})	$k'_{-p\text{-Ets-}F}$ (s^{-1})	$K'^{p\text{-Ets-}F}_d$ (μM)
9.4 ± 0.3^a	121 ± 3.8^a	$12.8 \pm 0.6^{a,b}$ 4.8 ± 0.5^c	6.2 ± 0.2^d 8.2 ± 0.1^e	123 ± 3^d 104 ± 2^e	$19.8 \pm 0.7^{b,d}$ 12.6 ± 0.6^b

[a]With 20 mM Mg^{2+}. [b]Calculated from k_1 and k_{-1}. [c]Determined by fluorescence anisotropy. [d]With 20 mM Mg^{2+} and 2 mM ADP. [e]With 20 mM Mg^{2+} and 4 mM ADP.

reasonable agreement with the $K_d^{p\text{-Ets-}F}$ value of 4.8 ± 0.5 μM determined by the anisotropy measurements in the presence of 1.3% glycerol. The presence of a saturating ADP concentration has only a marginal effect on these values (Table 2), providing further support for the notion that *p*-Ets and ADP do not interact energetically while bound to ERK2.

Determining the Rate of ADP Release. To investigate the mechanism of release of ADP from ERK2, we first determined its affinity by isothermal titration calorimetry. Figure 5 shows a typical titration where a change in the heat of the solution that accompanies the addition of MgADP to ERK2 (263 μM) signifies binding between the two molecules. Integration of the experimental isotherm using a single-site binding model established a dissociation constant K_d^{ADP} of 172 ± 6 μM for ADP with a binding stoichiometry of 1.02 ± 0.01 (Figure 5). This value is in excellent agreement with the parameters determined from the analysis of the reaction in the reverse direction (Table 1).

To investigate the rate of release of ADP from ERK2, we performed a trapping experiment, which allows measurement of individual points for a reaction time course on the millisecond to second time scale. The trapping approach has previously been used to estimate the rate of release of ATP and ADP from protein kinase complexes (*33*−*37*). An assumption is that the rate of release of ADP from the abortive complex, $E_{p\text{-Ets}}^{ADP}$, represents a good approximation of its rate of release from ERK2 during turnover. This appears to be a reasonable assumption, because as noted above there is little kinetic or thermodynamic evidence to suggest that the protein and nucleotide ligands interact significantly while bound to ERK2 (see Table 1). The approach depends on the ability to couple the rate of release of ADP from the $E_{p\text{-Ets}}^{ADP}$ abortive complex to a measurable signal. In the case of the experimental design shown in Scheme 4A, this signal is the formation of product (e.g., *p*-Ets).

As part of the trapping approach, two experiments were performed. In the first experiment (control experiment), ADP was mixed at the same time as ATP and Ets. In the second experiment (pre-equilibrium experiment), ERK2 was pre-incubated with ADP before the addition of Ets and ATP.

(*i*) *Control Experiment*. Figure 6B depicts a typical time course for the formation of *p*-Ets obtained at 5 μM ERK2 (final concentration) in the presence of 1 mM ADP and 5 mM ATP. In this experiment, ERK2 was rapidly mixed with an equal volume of a second solution containing ATP (10 mM), ADP (2 mM), and Ets (300 μM) (○). After a designated period (2−150 ms), reactions were quenched with acid via a second mixing event. Labeled *p*-Ets was then recovered and quantified after calibration of the machine as described previously (*24*). This time course is characterized by an initial burst followed by a slower, linear phase which may be described by the kinetic model shown in Scheme 4B (*24*). According to this model, the binding of ATP and

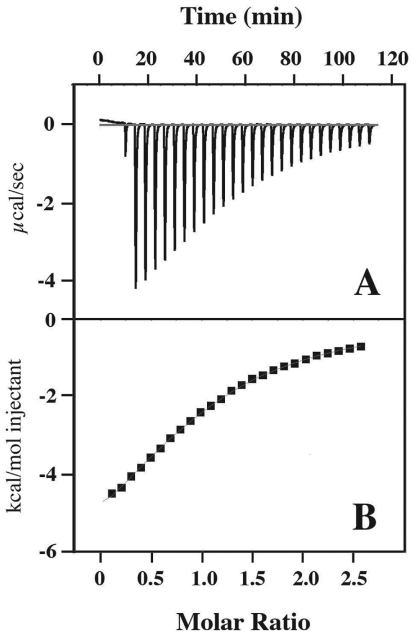

FIGURE 5: Isothermal titration calorimetric analysis of ADP binding to active ERK2. Titrations were conducted on a MCS titration calorimeter (Microcal, Inc.) at 27 °C in 25 mM HEPES (pH 8.0), 100 mM KCl, 2 mM β-mercaptoethanol, and 20 mM $MgCl_2$. *(A) Titration of MgADP (25 × 10 μL) into activated ERK2 (263 μM) at 27 °C. The concentration of the MgADP solution was such that a 2.5 molar ratio of MgADP to active ERK2 would be reached in the cell upon the last injection. (B) Integrated enthalpy change for each injection.

Scheme 4: (A) ERK2 and ADP Are Pre-Incubated To Form the Binary Complex E^{ADP}, before Being Rapidly Mixed with ATP and Ets, and (B) ERK2 Is Mixed with ATP, ADP, and Ets

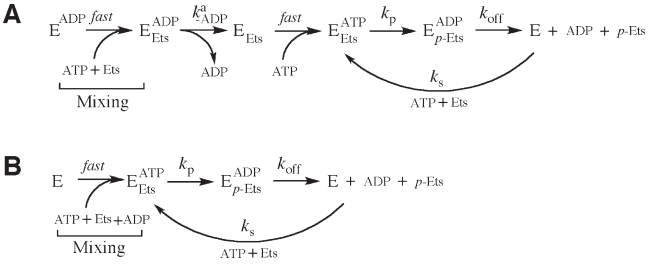

Ets to ERK2 is assumed to be fast and irreversible under the conditions employed. Thus, the reaction rate is dependent on two irreversible steps: the rate of product formation on the enzyme, k_p, and the rate of release of the product from the enzyme, k_{off}. According to this model, the observed rate of turnover is a function of the steady-state concentration of the ternary complex and is related to the slope of the linear phase of the reaction. On the basis of the K_d^{ADP} of 172 μM for ADP and the K_i^{ATP} of 65 μM for ATP (*20*), it may be estimated that under steady-state conditions >90% of ERK2 will be in a complex with ATP, with less than 10% in a complex with ADP. Consistent with this estimation, a comparison with previous experiments performed in the absence of ADP (*24*) suggests that the ADP in the trapping experiment has little effect on the steady-state rate under the experimental conditions.

(*ii*) *Pre-Equilibrium Experiment*. After determining that 1 mM ADP has a minimal effect on the rate of ERK2 in the presence of 5 mM ATP, we examined the effect of pre-incubating ADP (2 mM) with ERK2 (10 μM) before rapidly mixing them with ATP (10 mM) and Ets (300 μM). Syringe A contained ERK2 (10 μM) and ADP (2 mM). On the basis of the K_d^{ADP} of 172 μM established by the isothermal titration calorimetry experiment, 92% of ERK2 is expected to be complexed with ADP in syringe A. Syringe B contained both ATP (10 mM) and Ets (300 μM), whose rapid binding to ERK2 has been established previously: binding occurs with apparent association rates in excess of 400 s^{-1} at 150 μM Ets and 2 mM ATP (*24*). In contrast to a "burst phase" that precedes the linear phase in the control experiment, an initial lag phase is observed, which precedes the linear steady-state phase. The data in Figure 6A were analyzed using KinTek Explorer Pro (*25*, *26*), according to Scheme 4A, yielding the following rate constants: $k^a_{-ADP} = 61 \pm 13\ s^{-1}$, $k_p = 105 \pm 30\ s^{-1}$, and $k_{off} = 85 \pm 20\ s^{-1}$ (in good agreement with previously determined values, $k_p = 106 \pm 8\ s^{-1}$ and $k_{off} = 59 \pm 6\ s^{-1}$).

Toward a Structural Understanding of Catalysis: A Model of the ERK2−Ets-1 Interaction. Modeling for Interactions of ERK2 with Ets Residues 28−138. To gain insight into how ERK2 binds Ets-1, we sought to predict how the SAM domain of Ets-1 and ERK2 might interact. Toward this end, a complex structure consisting of active ERK2 (PDB entry 2ERK) and residues 28−138 of Ets-1 (PDB entry 2JV3) was predicted using the molecular mechanics modeling approaches available in TINKER (*28*), as described in Experimental Procedures. A feature of the predicted complex (Figure 7) is an interaction between loop 13 and helix αG of ERK2 with the helix 4−loop−helix 5 locus of the SAM domain of Ets-1. The general features of the model appear to be quite robust as they were predicted using several different approaches (e.g., different starting points and constraints).

To provide experimental support for the model, Lys-229 and His-230 of loop 13 were simultaneously mutated to Thr and Asp, respectively, the corresponding residues in p38 MAPK, a MAPK that binds Ets-1 weakly.[8] The K229T/H230D mutant was expressed, purified, and fully activated in the same manner as the wild-type enzyme. Activation was confirmed by mass spectrometric analysis, which showed that ~2 mol/mol of phosphate was incorporated into the protein by MKK1G7b (a constitutively active form of MKK1) and that only one radiolabeled peptide of the correct mass (corresponding to residues 178−196) was observed following trypsinization of the activated protein (data not shown). When examined in a kinase assay, the mutant displayed a 44-fold decrease in the specificity constant, k_{cat}/K_m, toward the Ets protein ($k_{cat} = 4.2 \pm 0.5$, and $K_m = 82.0 \pm 20$), suggesting that this locus mediates an important interaction between ERK2 and Ets-1, in support of the predicted model. We consider it unlikely that the mutations in these residues cause a global structural change because the ATPase activity of the mutant is comparable to that of the wild-type enzyme (data not shown).

DISCUSSION

Reverse Kinetics. Previous transient kinetic studies showed that product release partially limits the rate of Ets turnover by ERK2 (*24*); however, these studies did not identify which product dissociation step limits turnover. As *p*-Ets binds ERK2 some 20-fold more tightly than ADP (Tables 1 and 2), it was of interest to examine whether this translated to a slower rate of product release. This question is pertinent, because ERK2 has a number of diverse substrates, so it is of interest to determine how ERK2 and its substrates have coevolved to maximize the efficiency of

[8]Unpublished observations.

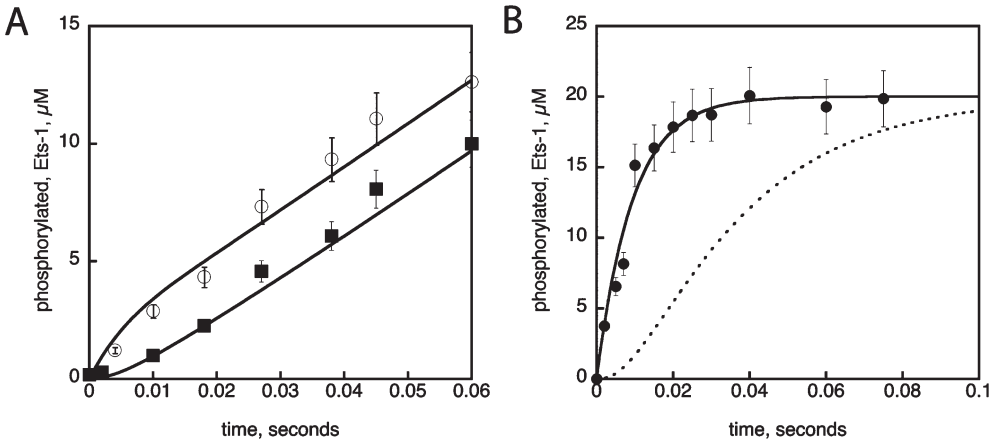

FIGURE 6: (A) Burst experiments in the presence of ADP. Rapid quench-flow experiments were conducted at 27 °C and pH 7.5 in buffer A (25 mM HEPES, 50 mM KCl, 2 mM DTT, 0.1 mM EDTA, and 0.1 mM EGTA) containing 20 mM $MgCl_2$. Sample loop A was loaded with [γ-^{32}P]ATP (100−1000 cpm/pmol) and ADP [0 (■) and 2 mM (○)], while sample loop B was loaded with Ets, ERK2, and ADP [2 (■) and 0 mM (○)]. Final concentrations were as follows: 5 mM MgATP, 1 mM MgADP, 150 μM Ets, and 5 μM ERK2. At set times, reactions were quenched by the addition of 2 M H_3PO_4 and product formation was quantified as described in Experimental Procedures. The lines through the data correspond to the best fit by numerical integration to Scheme 4A,B ($k^a_{ADP} = 61 \pm 13\ s^{-1}$, $k_p = 105 \pm 30\ s^{-1}$, and $k_{off} = 85 \pm 20\ s^{-1}$). (B) Single turnover. Rapid quench-flow experiments were conducted at 27 °C and pH 7.5 in buffer A (25 mM HEPES, 50 mM KCl, 2 mM DTT, 0.1 mM EDTA, and 0.1 mM EGTA) containing 20 mM $MgCl_2$. Sample loop A was loaded with [γ-^{32}P]ATP (100−1000 cpm/pmol), while sample loop B was loaded with Ets and ERK2. Final concentrations were as follows: 5 mM MgATP, 20 μM Ets, and 136 μM ERK2 (●). The line through the data corresponds to the best fit by numerical integration to Scheme 1, where $k_p = 106 \pm 8\ s^{-1}$. The dashed line corresponds to the predicted formation of product following rapid mixing, according to the iso random bi-bi mechanism and parameters reported by Wang et al. (*41*).

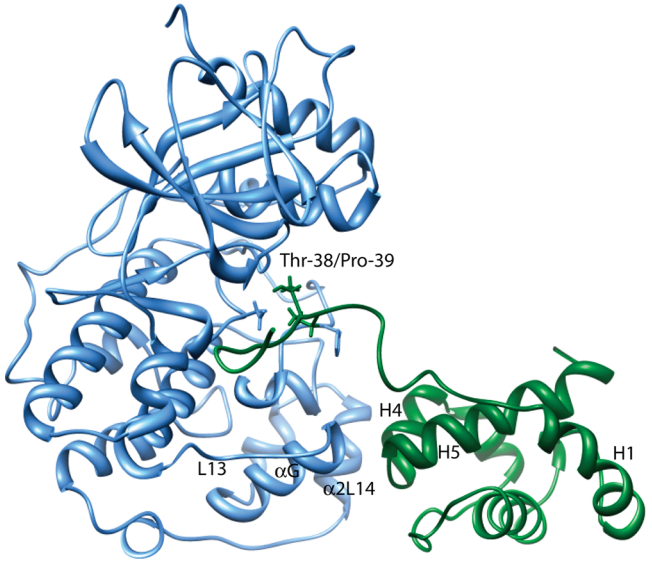

FIGURE 7: Modeling for interactions of ERK2 with Ets residues 28−138. The complex structure of active ERK2 (PDB entry 2ERK) and Ets (PDB entry 2JV3) was predicted as described in Experimental Procedures.

substrate turnover. One prediction is that, given that ADP release is a common step regardless of which substrate is being phosphorylated by ERK2, ADP release should at least be partially rate-limiting in cases where substrate turnover is efficient.

To investigate the process of product release, we first decided to examine the reaction in the reverse direction. This has the potential to provide information about the nature of product interactions as well as the order of product binding. On the basis of a previous examination of the reaction in the forward direction, we knew the reverse reaction must occur through a sequential mechanism (*31*) (Scheme 2). From the kinetic analysis of ATP formation shown in Figure 2, we determined that the magnitude of the catalytic constant for the reverse reaction, k^r_{cat}, is 0.2 s^{-1}. This value is significantly smaller than the anticipated

Scheme 5: Reaction Equilibria

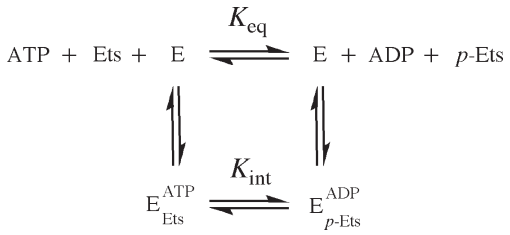

rate constant for the release of either ATP or Ets (the products of the reverse reaction) (*38*), suggesting that steps associated with the interconversion of the ternary complexes, k_{-p}, and not ATP or Ets release are likely to be rate-limiting in the reverse direction. Furthermore, as the rate of binding of ADP and *p*-Ets is considerably faster than k^r_{cat}, the reaction must occur through a rapid equilibrium mechanism in the reverse direction. Therefore, an ordered mechanism of ADP and *p*-Ets binding may be excluded on the basis of the fact that neither of the double-reciprocal plots for the reverse reaction in panels A and B of Figure 2A intersects on the *y*-axis (*31*). The data are therefore consistent with a rapid equilibrium random-order ternary complex mechanism for the reaction in the reverse direction. Accordingly, when the data in Figure 2 were fit to eq 1, kinetic parameters for the reaction (according to Scheme 2) were obtained (please see Table 1). These kinetic parameters suggest that, in the presence of 10 mM Mg^{2+}, little interaction occurs between ADP and *p*-Ets upon binding ERK2, with *p*-Ets binding some 20-fold more tightly than ADP.

$$K_{eq} = k^f_{cat} K^{ADP}_d K^{p\text{-Ets}}_m / k^r_{cat} K^{ATP}_i K^{Ets}_m \quad (9)$$

By examining the reaction in the reverse direction, we are able to use the Haldane relationship (eq 9) to estimate an equilibrium constant K_{eq} of 250 for the reaction in solution (Scheme 5). This value is smaller than the K_{eq} reported for the reaction between ATP and two peptides, Ac-LRRASLG (*39*) and PLARTLSVAGLPGKK (*40*), suggesting that sequence

and/or protein structure may influence the equilibria. Interestingly, the magnitude of the equilibrium for Thr-38 phosphorylation by ATP on ERK2 may be estimated by taking the ratio of the rate of phosphoryl transfer in the forward and reverse directions. In the forward direction, a rate constant k_p of 105 s^{-1} was determined from single-turnover experiments (*24*). In the reverse direction, a rate constant k^r_{cat} of 0.2 s^{-1} may be attributed to phosphoryl transfer, k_{-p}. These values predict an equilibrium K_{int} of 105/0.2 (= 525), indicating that K_{eq} and K_{int} are almost identical (Scheme 5).

Product Release. We found that the fluorescent protein *p*-Ets-*F* binds ERK2 with an affinity similar to that of the Ets protein (Figure 3A), and therefore, we used it to assess the mechanism of *p*-Ets binding in transient kinetic experiments. Analysis of the kinetic transients shown in Figure 4 by global fitting suggests that *p*-Ets-*F* binds ERK2 through a single-step mechanism with the following rate constants: $k_{p\text{-Ets-}F} = (9.4 \pm 0.3) \times 10^6$ M^{-1} s^{-1} and $k_{-p\text{-Ets-}F} = 121 \pm 3.8$ s^{-1} for association and dissociation, respectively. Similar results were obtained when ERK2 was pre-incubated with a saturating concentration of ADP (Table 2). Interestingly, the rate constant for *p*-Ets-*F* dissociation, $k_{-p\text{-Ets-}F}$, is approximately twice the magnitude of k_{off}, suggesting that Ets has indeed evolved to facilitate rapid dissociation. While we consider $k_{-p\text{-Ets-}F}$ to be a reasonable approximation to $k_{-p\text{-Ets}}$ as both *p*-Ets-*F* and *p*-Ets bind ERK2 with similar affinities (Table 2), the possibility that the rates of dissociation may be significantly different cannot be excluded. The similarity in the kinetic mechanism and magnitude of the parameters for the binding of *p*-Ets-*F* to ERK2 and the ERK2·ADP binary complex support the contention that Ets does not significantly interact with ADP upon binding. This also argues against a mechanism in which a rate-limiting conformational change precedes the release of the products, because such a step should be apparent upon the binding of *p*-Ets-*F* to the binary complex.

To assess the rate of release of ADP from ERK2, we turned to a trapping technique used previously to examine the release of ADP from other protein kinases (*33*−*36*). This technique relies on the ability of excess ATP and substrate to trap the enzyme as a productive ternary complex following rapid mixing with the enzyme, which had been pre-equilibrated with ADP and provides a value for k^a_{-ADP} (Scheme 4A). Figure 6A shows an experiment in which ADP was either pre-incubated with ERK2 or added at the same time as ATP. A comparison of experiments A and B shows clearly that pre-incubation with ADP abolishes the burst phase and introduces a lag phase without altering the magnitude of the steady-state linear phase. A global fit of the data to the mechanisms in panels A and B of Scheme 5 using numerical integration provided a good minimized fit and the following rate constants: $k^a_{-ADP} = 61 \pm 13$ s^{-1}, $k_p = 105 \pm 30$ s^{-1}, and $k_{off} = 85 \pm 20$ s^{-1}.

Taken together, these data support the notion that the Ets protein has evolved to interact in such a manner with ERK2 that both its phosphorylation and dissociation are comparable in rate to ADP dissociation. Recently, an iso random bi-bi mechanism was proposed for the phosphorylation of Ets by ERK2 (*41*) to account for the observed effects of addition of viscosogens to the steady-state reaction mixture. According to the mechanism, an isomerization step is partially rate-limiting; however, this would appear to be inconsistent with the observed kinetic data. For example, the iso random bi-bi mechanism predicts a lag in the formation of *p*-Ets under single-turnover conditions, which is clearly not the case in Figure 6B (dotted line). While we cannot explain the reason for the discrepancy, we note that the effect of viscosogens on the properties of proteins is often very difficult to predict.

Recognition of Ets-1 by ERK2. It is of interest to understand how Ets binds ERK2 to facilitate the efficient and specific phosphorylation of Thr-38. Enzymes have evolved under selective pressure to facilitate cellular processes, and ERK2 has the formidable task of phosphorylating a specific subset of cellular proteins (perhaps as many as 100) with a relatively high specificity constant (typically ~10^6 M^{-1} s^{-1}). Thus, an important broader goal is to determine distinguishing features of ERK2−substrate interactions. To address these issues and to provide a possible structural basis for the mechanism of Ets-1 phosphorylation, we examined the complex formed between activated ERK2 and residues 28−138 of Ets-1 (Figure 7).

To build the model, we began with a recent structure of CDK2/cyclin A3 bound to the optimal peptide substrate HHASPRK, which reveals how CDK2/cyclin A3 binds the P + 1 proline (*42*). Like ERK2, CDK2 is a proline-directed protein kinase. A characteristic feature of the P + 1 pocket of CDK2 is the unusual left-handed conformation of Val-164 (φ = 72.5°, and ψ = 130.8°), whose backbone carbonyl is oriented away from the opening of the pocket toward an arginine that is exclusively conserved in proline-directed kinases (Arg-169 in CDK2). Given the similarity of the conformation of the activation segments of ERK2 and CDK2, these enzymes are expected to bind the P + 1 proline in a similar manner. Therefore, the model was built by fixing Thr-38 and Pro-39 of Ets-1 at the active site of ERK2 according to the CDK2−peptide structure, before allowing the structure to relax.

The modeling predicts an interaction between the helix 4−loop−helix 5 portion of the SAM domain of Ets-1 and the loop 13−helix αG motif of ERK2 (Figure 7). This predicted interaction is consistent with previous mutagenesis studies of Ets-1 in which residues Leu-114 and Phe-120, which lie in the loop between H4 and H5, were shown to compromise the ability of ERK2 to phosphorylate Ets-1 both in vitro and in cells (*17*). Furthermore, several years ago, hypothesizing that MAPKs are related through gene duplication, Caffrey et al. performed a computational analysis to predict regions of functional difference between subfamilies of MAPKs (*43*). They reasoned that after gene duplication, a region of a protein that confers a functional difference between subfamilies, such as specificity, undergoes a physicochemical change and then conserves this change among members of the subfamily. When they compared the primary sequences of the MAPKs and searched for regions among subfamily members that significantly changed after gene duplication but remained conserved among subfamily members thereafter, they identified five regions of interest.[9] One region corresponded to residues Lys-229 and His-230, which lie at the end of loop 13 of ERK2. These residues appear to be important for the recognition of a number of ligands to ERK2, including MAPKK1 (*44*), phosphoprotein enriched in astrocytes-15 kDa (PEA-15) (*45*), MAPK phosphatase 3 (MKP3), and Elk-1 (*46*).

[9]A computational study was conducted by Caffrey et al. to predict regions of MAPKs conferring specificity differences among the MAPK subfamily members (*40*). Residues identified in this study fall into five loci on the surface of ERK2: (#1: His-59, Tyr-62, Gln-64, Leu-67), (#2: Tyr-111, Lys-112, Cys-125, Leu-154, Thr-157, Thr-158), (#3:Glu-184), (#4: Lys-201, Gly-202, Lys-205, and Ser-206), and (#5: Lys-229, His-230).

Scheme 6: Kinetic Model for the Phosphorylation of Ets by ERK2[a]

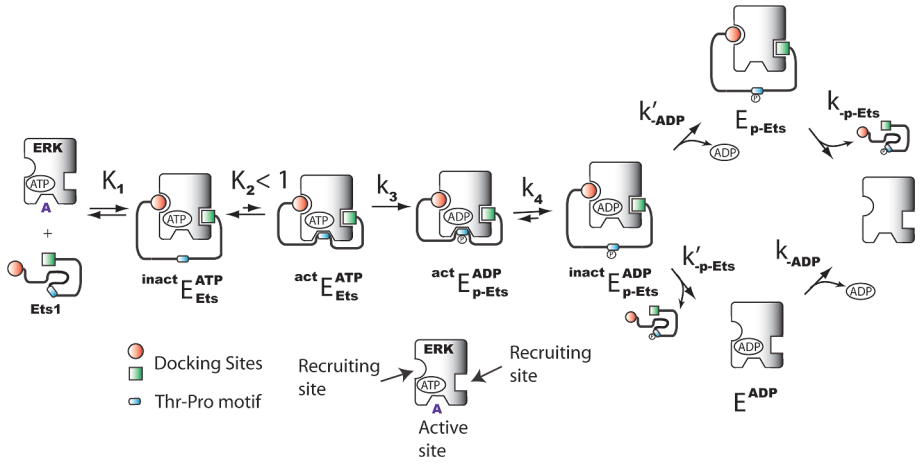

[a]ERK2 rapidly binds Ets to form an initial complex $^{inact}E^{ATP}_{Ets}$, which is catalytically incompetent, because the Thr-38-Pro-39 motif does not occupy the active site. This complex is mediated by the SAM domain as well as residues in the highly flexible N-terminus (*21*). We propose that $^{inact}E^{ATP}_{Ets}$ is on the reaction pathway for phosphoryl transfer to Thr-38 and that it undergoes an isomerization, to form the activated ternary complex $^{act}E^{ATP}_{Ets}$, which in contrast to $^{inact}E^{ATP}_{Ets}$ is catalytically competent because it is characterized by the binding of the Thr-Pro motif within the active site in such a manner that Thr-38 can form a hydrogen bond to the catalytic base, Asp-147, priming it for phosphoryl transfer, k_3, to form $^{act}E^{ADP}_{p\text{-}Ets}$, which then undergoes a conformational change, k_4, to form $^{inact}E^{ADP}_{p\text{-}Ets}$. Product dissociation occurs through a random-order mechanism. Abbreviations: $^{inact}E^{ATP}_{Ets}$, inactive conformation of the ternary complex E^{ATP}_{Ets}; $^{act}E^{ATP}_{Ets}$, active conformation of the ternary complex $^{act}E^{ATP}_{Ets}$; $^{inact}E^{ADP}_{p\text{-}Ets}$, inactive conformation of the ternary complex $E^{ADP}_{p\text{-}Ets}$; $^{act}E^{ADP}_{p\text{-}Ets}$, active conformation of the ternary complex $E^{ADP}_{p\text{-}Ets}$; K_1, association constant for the formation of the inactive ternary complex $^{inact}E^{ATP}_{Ets}$; K_2, equilibrium constant for the formation of $^{act}E^{ATP}_{Ets}$ from $^{inact}E^{ATP}_{Ets}$; k_3, first-order rate constant for the formation of $^{act}E^{ADP}_{p\text{-}Ets}$ from $^{act}E^{ATP}_{Ets}$; k_4, first-order rate constant for formation of $^{inact}E^{ADP}_{p\text{-}Ets}$ from $^{act}E^{ADP}_{p\text{-}Ets}$; k'_{-ADP}, first-order rate constant for the dissociation of ADP from $^{inact}E^{ADP}_{p\text{-}Ets}$; $k'_{-p\text{-}Ets}$, first-order rate constant for the dissociation of *p*-Ets from $^{inact}E^{ADP}_{p\text{-}Ets}$.

When we tested the ability of the K229T/H230D mutant to phosphorylate Ets, the mutant exhibited a 44-fold decrease in k_{cat}/K_m compared to that of wild-type ERK2, lending support to our model.

Mechanism. A feature of our model is that compared to unbound Ets-1, helix 1 (H1) of the SAM domain unwinds significantly to accommodate the binding of the Thr-38-Pro-39 motif in the active site. This is interesting, because our studies have suggested that the binding of the Thr-Pro motif in the active site of ERK2 may not be a feature of the ground-state ternary complex, but rather a feature of an intermediate along the reaction pathway (*21*, *23*). It is possible, for example, that the unfavorable cost of unwinding H1 could offset the favorable energy associated with the appropriate Thr-Pro binding to ERK2. While the model does not address how the N-terminus of Ets-1 (residues 1−27) binds to ERK2, experimental evidence suggests that it may interact within the DRS of ERK2 (*21*, *22*).

On the basis of the current and previous data (*21*, *22*), we propose a kinetic mechanism for the phosphorylation of Ets-1 in which, following docking, Thr-38 becomes localized within the proximity of the ERK2 active site in a ground-state ternary complex, $^{inact}E^{ATP}_{Ets}$ (Scheme 6). Two discrete docking sites found in the SAM domain and the N-terminus of Ets-1 span Thr-38 and stabilize this complex through interactions with the MAPK insert and the DRS, respectively. Accordingly, the ground-state complex then rearranges (K_2) to place the Thr-Pro motif in the active site primed for phosphorylation to give $^{act}E^{ATP}_{Ets}$. All steps following the formation of the ground-state ternary complex up to and including the phosphoryl transfer step correspond to k_p in Scheme 1, while all steps after the phosphorylation step contribute to k_{off}. Other features of the mechanism are that the dissociation of *p*-Ets from ERK2 is at least as fast as the dissociation of ADP and that products can dissociate in any order.

REFERENCES

1. Duesbery, N. S., Webb, C. P., and Vande Woude, G. F. (1999) MEK wars, a new front in the battle against cancer. *Nat. Med. 5*, 736–737.
2. Kohno, M., and Pouyssegur, J. (2006) Targeting the ERK signaling pathway in cancer therapy. *Ann. Med. 38*, 200–211.
3. Kohno, M., and Pouyssegur, J. (2003) Pharmacological inhibitors of the ERK signaling pathway: Application as anticancer drugs. *Prog. Cell Cycle Res. 5*, 219–224.
4. Milella, M., Kornblau, S. M., and Andreeff, M. (2003) The mitogen-activated protein kinase signaling module as a therapeutic target in hematologic malignancies. *Rev. Clin. Exp. Hematol. 7*, 160–190.
5. Sebolt-Leopold, J. S. (2000) Development of anticancer drugs targeting the MAP kinase pathway. *Oncogene 19*, 6594–6599.
6. Weinberg, R. A. (2006) The Biology of Cancer, Taylor & Francis, London.
7. Sivaraman, V. S., Wang, H., Nuovo, G. J., and Malbon, C. C. (1997) Hyperexpression of mitogen-activated protein kinase in human breast cancer. *J. Clin. Invest. 99*, 1478–1483.
8. Bos, J. L. (1989) ras oncogenes in human cancer: A review. *Cancer Res. 49*, 4682–4689.
9. Solit, D. B., Garraway, L. A., Pratilas, C. A., Sawai, A., Getz, G., Basso, A., Ye, Q., Lobo, J. M., She, Y., Osman, I., Golub, T. R., Sebolt-Leopold, J., Sellers, W. R., and Rosen, N. (2006) BRAF mutation predicts sensitivity to MEK inhibition. *Nature 439*, 358–362.
10. Thottassery, J. V., Sun, Y., Westbrook, L., Rentz, S. S., Manuvakhova, M., Qu, Z., Samuel, S., Upshaw, R., Cunningham, A., and Kern, F. G. (2004) Prolonged extracellular signal-regulated kinase 1/2 activation during fibroblast growth factor 1- or heregulin β1-induced antiestrogen-resistant growth of breast cancer cells is resistant to mitogen-activated protein/extracellular regulated kinase kinase inhibitors. *Cancer Res. 64*, 4637–4647.
11. Marampon, F., Ciccarelli, C., and Zani, B. M. (2006) Down-regulation of c-Myc following MEK/ERK inhibition halts the expression of malignant phenotype in rhabdomyosarcoma and in non muscle-derived human tumors. *Mol. Cancer 5*, 31.
12. Gysin, S., Lee, S. H., Dean, N. M., and McMahon, M. (2005) Pharmacologic inhibition of RAF→MEK→ERK signaling elicits pancreatic cancer cell cycle arrest through induced expression of p27Kip1. *Cancer Res. 65*, 4870–4880.
13. Brown, J. R., Nigh, E., Lee, R. J., Ye, H., Thompson, M. A., Saudou, F., Pestell, R. G., and Greenberg, M. E. (1998) Fos family members induce cell cycle entry by activating cyclin D1. *Mol. Cell. Biol. 18*, 5609–5619.

14. Eferl, R., and Wagner, E. F. (2003) AP-1: A double-edged sword in tumorigenesis. *Nat. Rev. Cancer 3*, 859–868.
15. Davies, H., Bignell, G. R., Cox, C., Stephens, P., Edkins, S., Clegg, S., Teague, J., Woffendin, H., Garnett, M. J., Bottomley, W., Davis, N., Dicks, E., Ewing, R., Floyd, Y., Gray, K., Hall, S., Hawes, R., Hughes, J., Kosmidou, V., Menzies, A., Mould, C., Parker, A., Stevens, C., Watt, S., Hooper, S., Wilson, R., Jayatilake, H., Gusterson, B. A., Cooper, C., Shipley, J., Hargrave, D., Pritchard-Jones, K., Maitland, N., Chenevix-Trench, G., Riggins, G. J., Bigner, D. D., Palmieri, G., Cossu, A., Flanagan, A., Nicholson, A., Ho, J. W., Leung, S. Y., Yuen, S. T., Weber, B. L., Seigler, H. F., Darrow, T. L., Paterson, H., Marais, R., Marshall, C. J., Wooster, R., Stratton, M. R., and Futreal, P. A. (2002) Mutations of the BRAF gene in human cancer. *Nature 417*, 949–954.
16. Biondi, R. M., and Nebreda, A. R. (2003) Signalling specificity of Ser/Thr protein kinases through docking-site-mediated interactions. *Biochem. J. 372*, 1–13.
17. Seidel, J. J., and Graves, B. J. (2002) An ERK2 docking site in the Pointed domain distinguishes a subset of ETS transcription factors. *Genes Dev. 16*, 127–137.
18. Qiao, F., and Bowie, J. U. (2005) The many faces of SAM. *Sci. STKE 2005* No. re7.
19. Waas, W. F., and Dalby, K. N. (2001) Purification of a model substrate for transcription factor phosphorylation by ERK2. *Protein Expression Purif. 23*, 191–197.
20. Waas, W. F., and Dalby, K. N. (2002) Transient protein-protein interactions and a random-ordered kinetic mechanism for the phosphorylation of a transcription factor by extracellular-regulated protein kinase 2. *J. Biol. Chem. 277*, 12532–12540.
21. Callaway, K. A., Rainey, M. A., Riggs, A. F., Abramczyk, O., and Dalby, K. N. (2006) Properties and regulation of a transiently assembled ERK2·Ets-1 signaling complex. *Biochemistry 45*, 13719–13733.
22. Abramczyk, O., Rainey, M. A., Barnes, R., Martin, L., and Dalby, K. N. (2007) Expanding the Repertoire of an ERK2 Recruitment Site: Cysteine Footprinting Identifies the D-Recruitment Site as a Mediator of Ets-1 Binding. *Biochemistry 46*, 9174–9186.
23. Rainey, M. A., Callaway, K., Barnes, R., Wilson, B., and Dalby, K. N. (2005) Proximity-induced catalysis by the protein kinase ERK2. *J. Am. Chem. Soc. 127*, 10494–10495.
24. Waas, W. F., Rainey, M. A., Szafranska, A. E., and Dalby, K. N. (2003) Two rate-limiting steps in the kinetic mechanism of the serine/threonine specific protein kinase ERK2: A case of fast phosphorylation followed by fast product release. *Biochemistry 42*, 12273–12286.
25. Johnson, K. A., Simpson, Z. B., and Blom, T. (2009) Global kinetic explorer: A new computer program for dynamic simulation and fitting of kinetic data. *Anal. Biochem. 387*, 20–29.
26. Johnson, K. A., Simpson, Z. B., and Blom, T. (2009) FitSpace explorer: An algorithm to evaluate multidimensional parameter space in fitting kinetic data. *Anal. Biochem. 387*, 30–41.
27. Peterman, B. F. (1979) Measurement of the dead time of a fluorescence stopped-flow instrument. *Anal. Biochem. 93*, 442–444.
28. Ponder, J. W. (2006) TINKER: Software Tools for Molecular Design, Washington University Medical School, St. Louis (http://dasher.wustl.edu/tinker/).
29. Jorgensen, W. L., Maxwell, D. S., and TiradoRives, J. (1996) Development and testing of the OPLS all-atom force field on conformational energetics and properties of organic liquids. *J. Am. Chem. Soc. 118*, 11225–11236.
30. Pappu, R. V., Marshall, G. R., and Ponder, J. W. (1999) A potential smoothing algorithm accurately predicts transmembrane helix packing. *Nat. Struct. Biol. 6*, 50–55.
31. Segel, I. H. (1993) Enzyme Kinetics: Behavior and Analysis of Rapid Equilibrium and Steady-State Enzyme Systems, Wiley Classics Library Edition, John Wiley & Sons, Inc., New York.
32. Callaway, K., Abramczyk, O., Martin, L., and Dalby, K. N. (2007) The anti-apoptotic protein PEA-15 is a tight binding inhibitor of ERK1 and ERK2, which blocks docking interactions at the D-recruitment site. *Biochemistry 46*, 9187–9198.
33. Keshwani, M. M., and Harris, T. K. (2008) Kinetic mechanism of fully activated S6K1 protein kinase. *J. Biol. Chem. 283*, 11972–11980.
34. Lieser, S. A., Shindler, C., Aubol, B. E., Lee, S., Sun, G., and Adams, J. A. (2005) Phosphoryl transfer step in the C-terminal Src kinase controls Src recognition. *J. Biol. Chem. 280*, 7769–7776.
35. Shaffer, J., Sun, G., and Adams, J. A. (2001) Nucleotide release and associated conformational changes regulate function in the COOH-terminal Src kinase, Csk. *Biochemistry 40*, 11149–11155.
36. Shaffer, J., and Adams, J. A. (1999) Detection of conformational changes along the kinetic pathway of protein kinase A using a catalytic trapping technique. *Biochemistry 38*, 12072–12079.
37. Kong, C. T., and Cook, P. F. (1988) Isotope partitioning in the adenosine 3′,5′-monophosphate dependent protein kinase reaction indicates a steady-state random kinetic mechanism. *Biochemistry 27*, 4795–4799.
38. Prowse, C. N., Hagopian, J. C., Cobb, M. H., Ahn, N. G., and Lew, J. (2000) Catalytic reaction pathway for the mitogen-activated protein kinase ERK2. *Biochemistry 39*, 6258–6266.
39. Qamar, R., Yoon, M. Y., and Cook, P. F. (1992) Kinetic mechanism of the adenosine 3′,5′-monophosphate dependent protein kinase catalytic subunit in the direction of magnesium adenosine 5′-diphosphate phosphorylation. *Biochemistry 31*, 9986–9992.
40. Kwiatkowski, A. P., Huang, C. Y., and King, M. M. (1990) Kinetic mechanism of the type II calmodulin-dependent protein kinase: Studies of the forward and reverse reactions and observation of apparent rapid-equilibrium ordered binding. *Biochemistry 29*, 153–159.
41. Wang, Z. X., and Wu, J. W. (2007) The complete pathway for ERK2-catalyzed reaction. Evidence for an iso random Bi Bi mechanism. *J. Biol. Chem. 282*, 27678–27684.
42. Brown, N. R., Noble, M. E., Endicott, J. A., and Johnson, L. N. (1999) The structural basis for specificity of substrate and recruitment peptides for cyclin-dependent kinases. *Nat. Cell Biol. 1*, 438–443.
43. Caffrey, D. R., O'Neill, L. A., and Shields, D. C. (2000) A method to predict residues conferring functional differences between related proteins: Application to MAP kinase pathways. *Protein Sci. 9*, 655–670.
44. Robinson, F. L., Whitehurst, A. W., Raman, M., and Cobb, M. H. (2002) Identification of novel point mutations in ERK2 that selectively disrupt binding to MEK1. *J. Biol. Chem. 277*, 14844–14852.
45. Chou, F. L., Hill, J. M., Hsieh, J. C., Pouyssegur, J., Brunet, A., Glading, A., Uberall, F., Ramos, J. W., Werner, M. H., and Ginsberg, M. H. (2003) PEA-15 binding to ERK1/2 MAPKs is required for its modulation of integrin activation. *J. Biol. Chem. 278*, 52587–52597.
46. Zhang, J., Zhou, B., Zheng, C. F., and Zhang, Z. Y. (2003) A bipartite mechanism for ERK2 recognition by its cognate regulators and substrates. *J. Biol. Chem. 278*, 29901–29912.